



Electrochemical analysis of graphene/Mo₉Se₁₁ nanocomposites towards energy storage application

V. Balasubramanian¹ · J. Celina Selvakumari¹ · J. Dhanalakshmi¹ · M. Ahila¹ · D. Pathinettam Padiyan¹

Received: 12 November 2017 / Accepted: 17 February 2018 / Published online: 26 February 2018
© Springer Science+Business Media, LLC, part of Springer Nature 2018

Abstract

This paper essentially analyses graphene/Mo₉Se₁₁ nanocomposites routes to supercapacitor applications which is one of the prominent devices for high power storage. Graphene and Mo₉Se₁₁ are coupled together by attrition followed by ultrasonification. The reduction of graphene oxide to graphene as well as the coupling of graphene with Mo₉Se₁₁ and the formation of their nanocomposites is confirmed through X-ray diffraction pattern, FTIR spectra and Raman spectra analysis of these materials. The surface morphology of the entire samples is imaged through SEM while their electrochemical performances are analysed by cyclic voltametry and electrochemical impedance spectroscopy. The nanocomposite, having three parts of Mo₉Se₁₁ and one part of graphene, displayed the higher areal capacitance of 438 mF at a scan rate of 5 mV s⁻¹. Finally, the solution resistance and charge transfer resistance are obtained from EIS measurements and reported.

1 Introduction

Supercapacitors (SCs), also called ultracapacitors, electrochemical capacitors, or electrical double-layer capacitors, are considered to be one of the most promising power sources for many portable systems and automotive applications, due to their high power density, fast charge–discharge rates, simple mechanism, and long life cycle [1–6]. In this study, graphene/Mo₉Se₁₁ nanocomposites synthesis and their application to high performance energy storage devices is reported. Usually carbon based materials such as carbon nanotubes, carbon nanofibres and graphene [7–10] are used as electrode material in SCs [11, 12]. Also transition metal dichalcogenides have emerged as one of the prominent

device for energy storage due to their unique crystal structure and material properties [13, 14].

Graphene is an atom-thick, two-dimensional (2D) material composed of a monolayer hexagonal *sp*² hybridized carbon. Graphene with the maximum surface area of 2630 m² g⁻¹ and high intrinsic electrical conductivity is believed to be one of the most promising electrode materials for SCs. However, in practical applications, graphene usually suffer from agglomeration or restacking due to strong van der Waals interactions, which leads to the loss of surface area and capacitance [15]. In this study, graphene is synthesized from graphene oxide (GO) by modified Hummer's method to improve its properties. Usually transition metal dichalcogenides (TMDC) materials are currently introduced into the interlayer of graphene to prevent agglomeration. TMDC, such as MoSe₂, WSe₂, MoS and WS have been recognized as the best electrode materials for SCs due to their capacitive behavior. However, their expensive nature and high toxicity severely limit their practical application in large scale synthesis [16, 17]. There are three possible methods to prepare GO namely Brodie, Hummer's and Staudenmeier. Brodie prepared graphite oxide using fuming conc. nitric acid, while Staudenmaier modified this method by replacing the role of nitric acid using conc. sulphuric acid. However, both these long methods were further modified by Hummer using conc. sulphuric acid along with potassium

✉ J. Dhanalakshmi
dhanam0610@gmail.com

V. Balasubramanian
abbala06@gmail.com

J. Celina Selvakumari
celinarathinam@yahoo.com

M. Ahila
ahilam.ahila@gmail.com

D. Pathinettam Padiyan
dppadiyan@gmail.com

¹ Department of Physics, Manonmaniam Sundaranar University, Tirunelveli, Tamil Nadu 627012, India

permanganate. Luo et al. [18] reported the GO and MoSe₂ nanopowders preparation using hydrazine hydrate as a reducing agent in order to make it as anode material having long cycle life for Li-ion batteries. Ma et al. [19] reported the synthesis of hierarchical MoSe₂/C hybrid with enhanced electrochemical performance for SC application using hydrothermal method. In the present work, graphene is synthesized via modified Hummer's method and Mo₉Se₁₁ is coupled together to form graphene/Mo₉Se₁₁ nanocomposite so as to improve their electrochemical performance. Moreover these materials have many advantages such as lightweight, high chemical resistance, high mechanical stability and ease of fabrication.

2 Experimental

2.1 Materials

Selenium metal powder (Se), sodium borohydride (NaBH₄), and sodium molybdate (Na₂MoO₄·2H₂O) was used for the synthesis of Mo₉Se₁₁ nanoparticles. Graphite powder, conc. sulphuric acid (H₂SO₄), potassium permanganate (KMnO₄), hydrogen peroxide (H₂O₂), and hydrochloric acid (HCl) was used for the synthesis of graphene. All the chemicals were purchased from Merck and Himedia. Throughout the experiment double distilled (DD) water was used.

2.2 Synthesis of graphene

Graphene was synthesized following modified Hummer's method [20, 21]. 1 g of graphite powder was added to 20 ml of con. sulphuric acid solution, with stirring over a period of 2 h. Solid KMnO₄ (3 g) was added slowly to the above solution, with continuous stirring and a reaction temperature of less than 20 °C was maintained. The mixture was then stirred at 35–40 °C for 30 min, followed by stirring at 65–80 °C for 30 min. The resulting solution was diluted by adding 25 ml of distilled water, and the mixture was heated at 90 °C for 30 min. The solution was dark brown in colour. On further stirring the dark brown color changed to black after 2 h. Then the mixture was further diluted by the addition of 75 ml of distilled water. 5 ml H₂O₂ was added slowly to the above solution. The precipitate was washed by repeated centrifugation and filtration, first with 5% HCl aqueous solution and then with distilled water, until the pH of the solution became neutral. Finally 75 ml of DD water was added to the resulting precipitate and sonicated for 1 h. The final product GO was dried in an oven and the obtained powder is named as GO. 50 mg of GO was dispersed in

100 ml of DD water, sonicated for 1 h to obtain graphene and labelled as G1.

2.3 Synthesis of Mo₉Se₁₁

15.7 mM selenium metal powder and 0.2 g of sodium borohydride were mixed in 50 ml of DD water under vigorous stirring until the solution became colourless. Precisely, 5.455 mM sodium molybdate was added to the NaBH₄ and Se mixture, followed by continuous stirring until a red solution was obtained [20]. Then the mixture was washed and filtered in order to get the precipitate. The precipitate was dried in an oven and the obtained Mo₉Se₁₁ nanoparticles are named as MO.

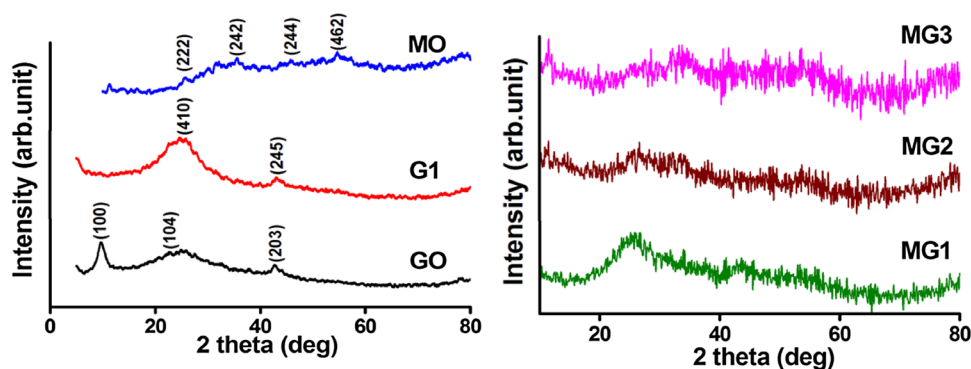
2.4 Synthesis of graphene/Mo₉Se₁₁ composites

In this study graphene/Mo₉Se₁₁ nanocomposites were synthesised via precipitation method. The synthesised Mo₉Se₁₁ nanoparticles were coupled with as synthesised graphene nanoparticles by grinding followed by ultrasonication. Three parts of graphene (300 mg) and one part of Mo₉Se₁₁ (100 mg) by weight were taken and grinded for 1 h to mix thoroughly. Next these composites were ultrasonicated for 1 h, centrifuged, dried at 80 °C for 1 h and named as MG1. Similarly the composites prepared with 200 mg of Mo₉Se₁₁ and 200 mg of graphene was named as MG2, while 1 part of graphene and three parts of Mo₉Se₁₁ composite was named as MG3.

2.5 Characterization

The structural properties of graphene/Mo₉Se₁₁ nanoparticles were characterized using XPERT-PRO diffractometer system. The X-ray radiation used was that emitted by copper, having characteristic wavelength of 1.5406 Å for the Kα radiation. The presence of vibrational modes of various functional groups was identified from the Fourier Transform Infra Red (FTIR) spectral analysis. The infrared absorption spectra of the prepared samples were measured at room temperature in the range of 4000–400 cm⁻¹ using Perkin Elmer FTIR spectrometer. The presence of vibrational, rotational and other low frequency modes were analyzed from the Raman spectra recorded in EZRaman-N Series Raman Analyzer with an excitation wavelength of 785 nm. The surface morphology studies were carried out using scanning electron microscope, JEOL Model JSM-639OLV at a potential of 20 kV. The electrochemical measurements were performed in a conventional three-electrode system using CH 1604E electrochemical workstation. Here, 1 M H₂SO₄ was used as the electrolyte, while the

Fig. 1 XRD patterns of GO, Graphene (G1), Mo₉Se₁₁ (MO), graphene/Mo₉Se₁₁ nanocomposites (MG1, MG2 and MG3)



working electrodes were prepared by mixing the electroactive material with polyvinyl alcohol and coated in an exactly 1 cm² active area. A large surface area platinum mesh and Ag/AgCl electrode were used as the counter and reference electrodes respectively. The electrochemical performance of the fabricated electrode was characterized by cyclic voltammetry (CV) and electrochemical impedance spectroscopy (EIS) measurements. The CV curves were recorded at various scan rates (5, 10, 50 and 100 mV s⁻¹) in a potential window of 0.8 to -0.5 V. The EIS measurements were carried out in the frequency range of 0.1 Hz to 100 kHz with an AC amplitude of 5 mV.

3 Results and discussion

Figure 1 displays the XRD patterns of GO, graphene, Mo₉Se₁₁ and graphene/Mo₉Se₁₁ nanocomposites of three different compositions. GO shows an intense X-ray peak at 9.6° assigned to (100) reflection and two weak and broad X-ray peak which corresponds to (104) and (203) reflections. The average crystallite size has been calculated using Scherrer formula [22] given by

$$D = 0.9\lambda / \beta \cos \theta \quad (1)$$

where λ is wavelength of the X-ray source, β is full width at half maximum and θ is diffraction angle. The crystallite size calculated using the intense X-ray peak is 6 nm.

After reduction, although the GO peak at 9.6° is completely disappeared in graphene, a strong intense peak of graphene appeared at 26.2° assigned to (410) reflection reveals the presence of water and oxygen containing group between the layers. The crystallite size of graphene is estimated as 5 nm. The reduction in crystallite size confirms that oxygen level has been reduced in G1 compared to GO. The other X-ray peaks observed at 22.7°, 42.8° corresponds to (104) and (203) reflections respectively. On reduction of GO, the hydroxyl, carbonyl and epoxide groups are bonded together and changed from *sp*² to *sp*³ bonds [23]. For Mo₉Se₁₁, five weak X-ray peaks are observed in which the high intense

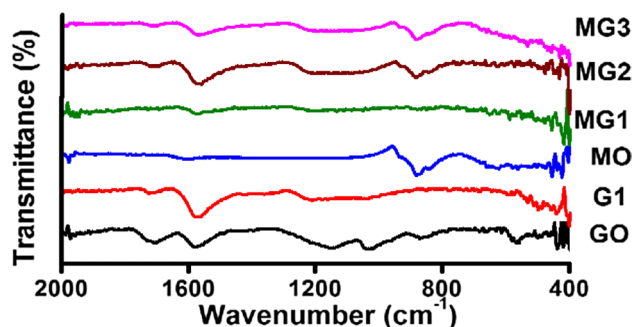


Fig. 2 FTIR spectra of GO, graphene (G1), Mo₉Se₁₁ (MO), graphene/Mo₉Se₁₁ nanocomposites (MG1, MG2 and MG3)

peak observed at 32.1° corresponds to (241) reflection and the crystallite size is 6 nm. The other peaks observed at 35.6°, 25.7°, 54.7° and 45.5° corresponds to (242), (222), (462) and (244) reflections respectively. In nanocomposites, MG1 sample shows that graphene X-ray peak is predominant than Mo₉Se₁₁, since graphene and Mo₉Se₁₁ is mixed in the ratio of 3:1, whereas in MG2 and MG3 the intensity of the graphene peak get reduced. Further no other X-ray peaks are observed in MG1, MG2 and MG3 revealing the amorphous nature of the composites.

The FTIR spectra of all the sample is shown in Fig. 2. The functional groups present in GO are hydroxyl (-OH)

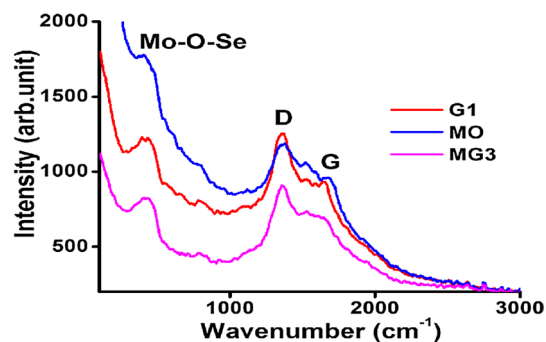


Fig. 3 Raman spectra of graphene (G1), Mo₉Se₁₁ (MO) and graphene/Mo₉Se₁₁ nanocomposite (MG3)

and epoxy ($-C-O-C$). For GO, the characteristic peak observed at 1562 cm^{-1} corresponds to $C=C$ stretching mode. The other bands related to oxygen containing functional groups such as epoxy and hydroxyl group seen at 1143 and 2683 cm^{-1} indicate the presence of oxygen in GO. In graphene (G1), the intensities of the peaks corresponding to oxygen containing functional groups get decreased revealing the removal of oxygen content, while the peak at 1562 cm^{-1} denote $C=C$ stretching have increase in intensity compared

to GO. In Mo_9Se_{11} , Mo and Se peaks are observed at 879 and 440 cm^{-1} respectively. The peaks seen at 1986 and 1600 cm^{-1} denotes the presence of carbonyl and absorption of water molecule. In nanocomposites, MG1 shows broad bands at 1562 and 854 cm^{-1} which confirm the presence of both the end members of graphene and Mo_9Se_{11} . In MG2, the strength of both the above peaks increased and it is attributed to the interaction between graphene and Mo_9Se_{11} . In MG3, the intensity of Mo_9Se_{11} peak increases

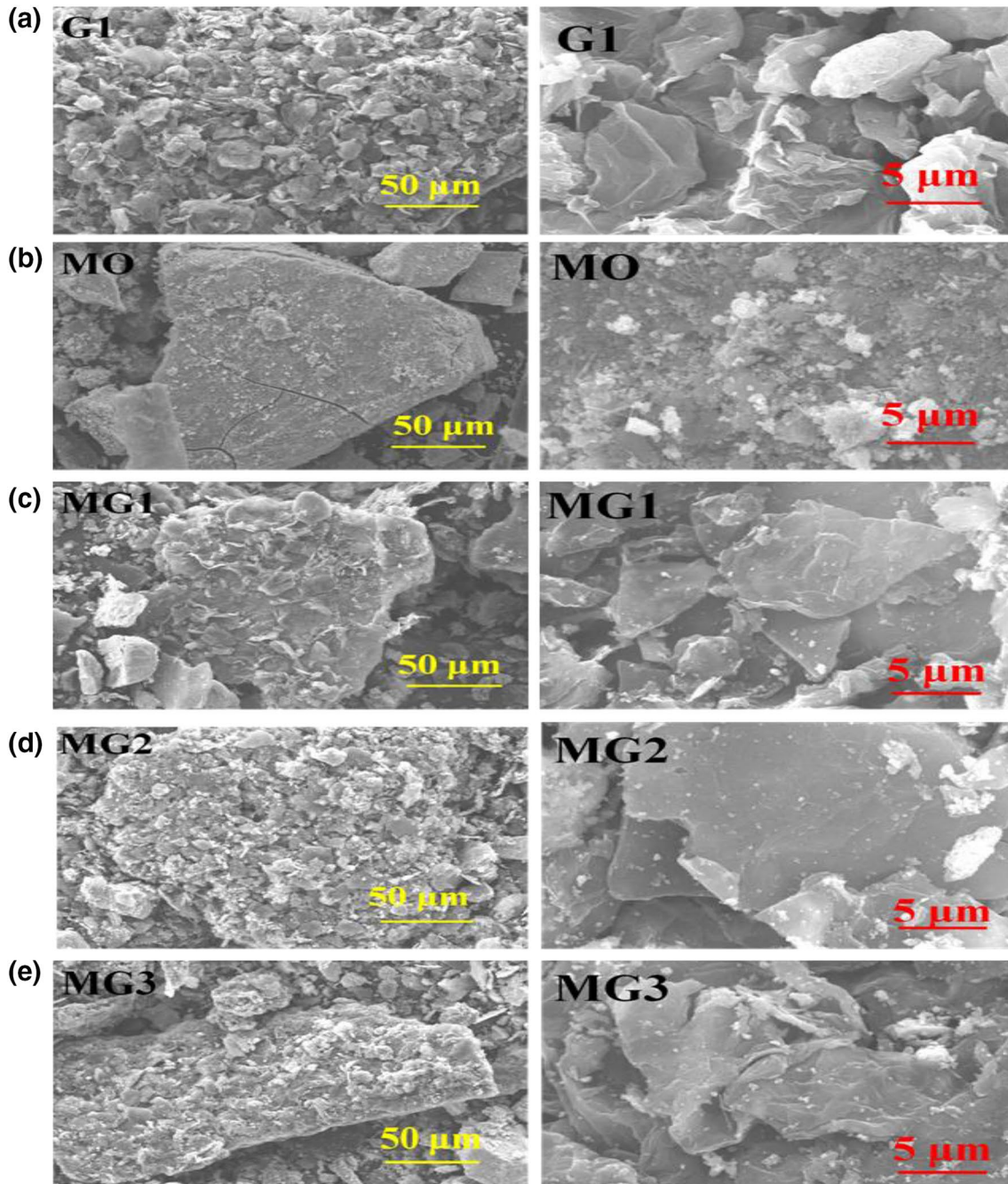
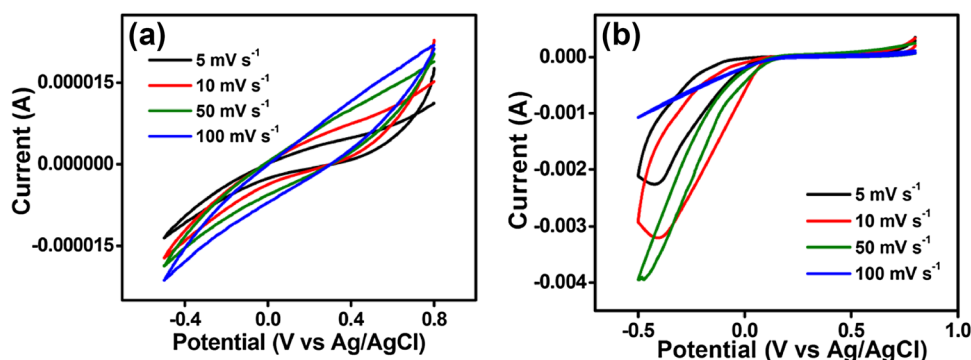


Fig. 4 SEM images of **a** graphene, **b** Mo_9Se_{11} , and graphene/ Mo_9Se_{11} nanocomposites **c** (MG1), **d** MG2, **e** MG3

Fig. 5 CV curve of **a** graphene and **b** Mo₉Se₁₁



whereas graphene peak get decreased. The variation of graphene and Mo₉Se₁₁ peak intensities confirmed the formation of chemical bonding between these two materials in the nanocomposites.

The Raman spectra of graphene, Mo₉Se₁₁ and its nanocomposite MG3 are shown in Fig. 3. The characteristic peaks of graphene appeared at 1349 and 1593 cm⁻¹ are assigned to D and G bands of graphene. The G band indicates the vibration of the sp² carbon atom in the two-dimensional hexagonal lattice, while the D band is related to the structural defects and disorder of the graphene [24]. Mo₉Se₁₁ characteristic peak seen at 449 cm⁻¹ denotes Mo, Se and O interactions.

In the nanocomposite MG3, the peak at 439, 1360 and 1604 cm⁻¹ corresponds to Mo–O–Se vibrations and D and G bands of graphene respectively. The peak correspond to Mo₉Se₁₁ get shifted towards the lower wavenumber region while graphene peaks are shifted towards the higher wave number region. The peak seen in Mo₉Se₁₁ at 437 cm⁻¹ is red shifted to 429 cm⁻¹ in nanocomposites, whereas, the D and G bands of graphene at 1349 cm⁻¹ is blue shifted to 1360 and 1598 cm⁻¹ respectively in MG3. This is due to the structural disorder of the material. The Raman D and G bands are comparatively less intense in the nanocomposite compared to graphene, which reveals the decrease in crystallinity and it is in agreement with the XRD analysis.

Figure 4 shows the SEM images of graphene, Mo₉Se₁₁ and its nanocomposites measured at two different magnifications. The morphology revealed that graphene (G1) looks like in the form of “corn flakes” with odd shape and size. In Mo₉Se₁₁, hard rock like surface is seen along with some rods on the surface of the particles. In MG1 nanocomposite, graphene flakes are mostly seen than Mo₉Se₁₁ rock like structure since graphene and Mo₉Se₁₁ are mixed in the ratio of 3:1. In MG2, both flakes and rocks are clearly seen due to equal proportion. In MG3, flakes are uniformly distributed on the surface of rocks like structure. The porous structure seen in these material will allow electrolyte penetration,

which is favourable for ion diffusion, charge transfer and capacitance increase.

Figure 5 shows the CV curve of graphene and Mo₉Se₁₁ measured at four different scan rates. The cyclic voltammogram of all the samples measured at various scan rate shows that as the scan rate increases the peak gets shifted towards the higher potential region. The areal capacitance of the as-prepared electrode is calculated from the CV curve using the following equation:

$$C_a = I / [dv/dt] \times S \rightarrow (F) \quad (2)$$

where C_a is the areal capacitance (F), I is the integrated area of the CV curve, dv/dt is the scan rate, S is the surface area of the electroactive material. In Mo₉Se₁₁, the integrated area of the CV curves is higher compared to graphene. At 5 mV s⁻¹, Mo₉Se₁₁ yields a better capacitance value of 79.20 mF, whereas in graphene it is 1.028 mF only. When the scan rate decreases, the capacitance value increases and Mo₉Se₁₁ yield a better capacitance value than graphene. A similar “electroactivation” process and increasing capacitance retention trend has been previously been reported in the graphene and MoS₂-based materials [25–29].

Figure 6 shows the CV curve for graphene/Mo₉Se₁₁ nanocomposites. Among the three composites, the sample MG3 shows the high capacitance value than MG1 and MG2. In MG3, a redox peak is observed at -0.19 V, whereas in MG2 and MG1, the redox peak is seen at 0.11 and 0.05 V respectively. As the scan rate increases, the capacitance value decreases in all the three nanocomposites. However, at all the scan rates, the sample MG3 shows the higher capacitance values. The sample MG3 has a higher integrated area in the CV curve compared to MG1 and MG2. MG3 displayed higher areal capacitance value of 438 and 255 mF at the scan rate of 5 and 10 mV s⁻¹ respectively. In MG2 and MG1 it has 7.32 and 3.32 mF respectively at 5 mV s⁻¹ scan rate. In MG3, as the scan rate increases the anodic peak get shifted towards the higher potential region, indicating the distortion in the material. At higher scan rate, the areal capacitance decreases and around 50% of the initial

Fig. 6 CV curves of graphene/ $\text{Mo}_9\text{Se}_{11}$ nanocomposites: **a** MG1, **b** MG2 and **c** MG3

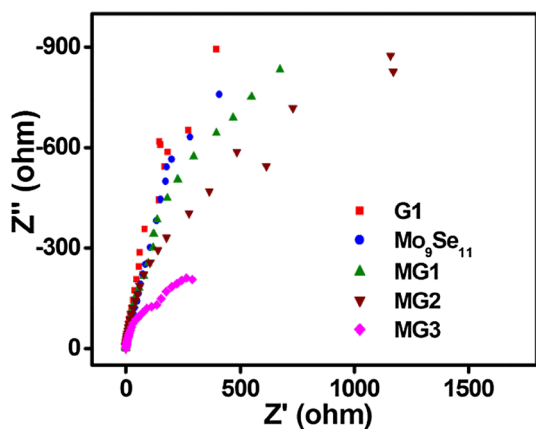
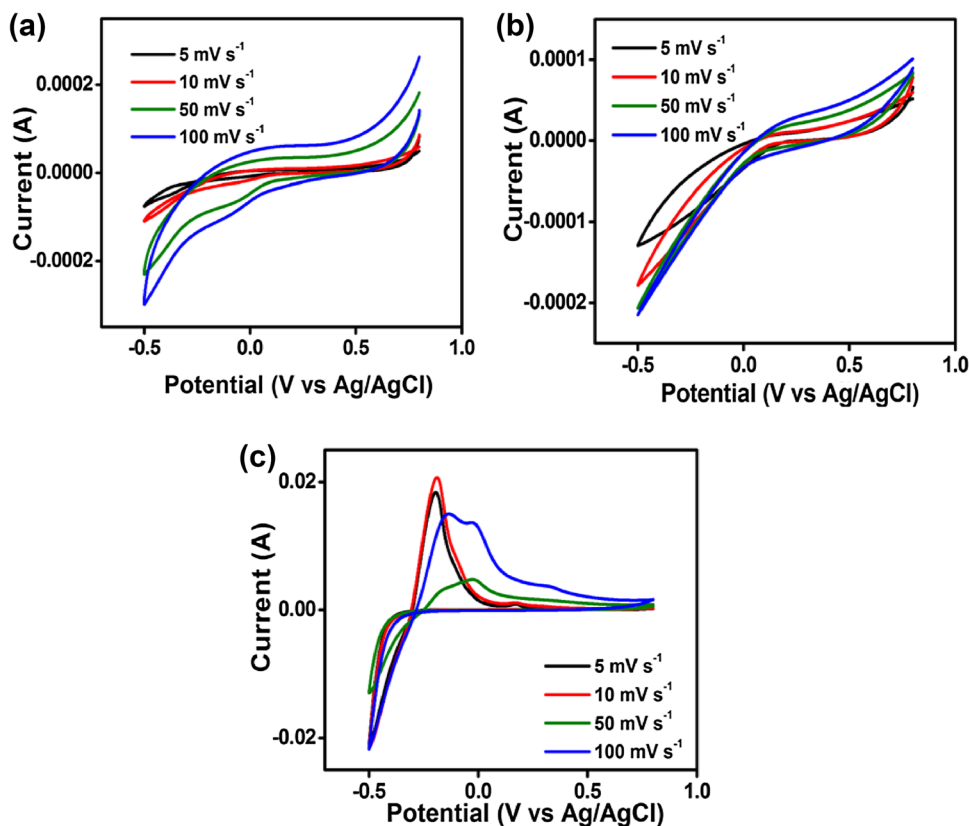


Fig. 7 Nyquist plot of graphene, $\text{Mo}_9\text{Se}_{11}$ and its nanocomposites

capacitance is retained. The sample MG3 shows the high areal capacitance at low scan rates and it is a better nanocomposite for SC application.

In order to further understand the fundamental electrochemical behavior of the as-prepared materials, EIS analyses were performed. In the Nyquist plot shown in Fig. 7, the x-intercept at the beginning of the semicircle represents the equivalent series resistance, including the electrolyte

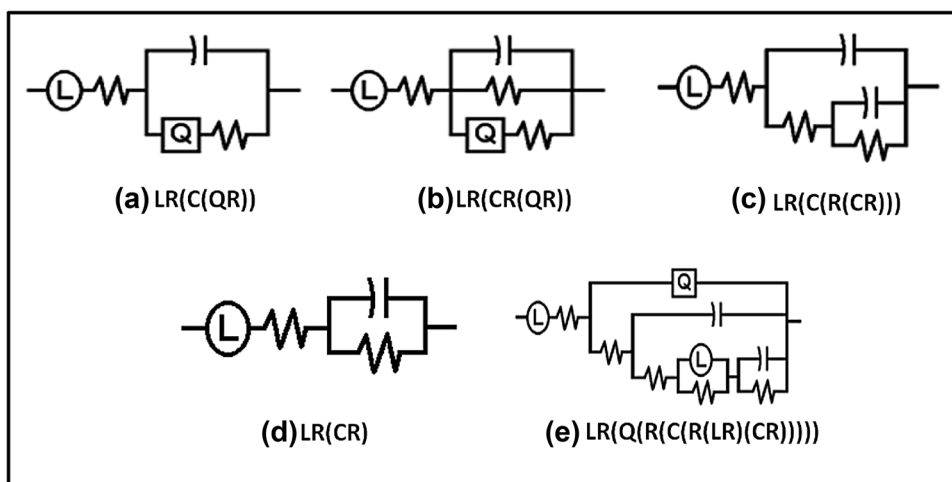
Table 1 Solution and charge transfer resistance of the samples

S. no.	Sample	R_s	R_{ct}
1	Graphene	0.07671	563.7
2	$\text{Mo}_9\text{Se}_{11}$	0.0927	98.43
3	MG1	0.07354	484.4
4	MG2	0.08149	548.2
5	MG3	0.00598	133.6

resistance, contact resistance at the interface between the electroactive material and substrate. The semicircle in the high frequency region is related to the charge transfer resistance (R_{ct}) at the electrode/electrolyte interface, and the inclined line at the beginning of semicircle corresponds to diffusive resistance of electrolyte ions inside the electrode materials [30, 31]. The solution resistance and the charge transfer resistance of the samples are given in Table 1 for comparison.

The corresponding equivalent circuit for all the samples is shown in Fig. 8. The sample MG3 shows the lowest R_s and R_{ct} value which indicates the higher conductivity and better charge transport of electrolyte ions, compared to graphene and $\text{Mo}_9\text{Se}_{11}$. Also in CV measurements, MG3 has

Fig. 8 Equivalent circuits of **a** graphene, **b** Mo₉Se₁₁, and graphene/Mo₉Se₁₁ nanocomposites **c** MG1, **d** MG2 and **e** MG3



higher areal capacitance value of 438 at the scan rate of 5 and 10 mV s⁻¹ compared to other composites. It is a better material for SC.

4 Conclusions

In summary, we have successfully synthesized Graphene and Mo₉Se₁₁ nanoparticles via modified Hummer's method and precipitation method. Both materials are coupled together by attrition for three different compositions to improve their properties and evaluated for SC applications. The XRD pattern reveals the reduction of GO to graphene with the presence of strong intense peak at 26.2° and it is well supported by Raman. The crystallite size of graphene, Mo₉Se₁₁ and their nanocomposites are in the range of 5–6 nm. In case of nanocomposites, the existence of both graphene and Mo₉Se₁₁ is confirmed from Raman and FTIR analysis. The surface morphology of the samples displayed the formation of rock like structure over which nano rods are seen. The enhanced electrochemical performance of graphene/Mo₉Se₁₁ nanocomposites are attributed to the interaction between graphene and Mo₉Se₁₁. Cyclic Voltammogram revealed that MG3 nanocomposite have a higher capacitance value of 438 mF at a scan rate of 5 mV s⁻¹. From impedance analysis, the solution resistance and charge transfer resistance of all the materials are obtained. These results suggest that graphene/Mo₉Se₁₁ nanocomposite has great potential for application in high performance SCs.

Acknowledgements We acknowledge Sophisticated Test and Instrumentation Centre, SAIF, CUSAT for SEM measurements and Noorul Islam University for Raman spectra recording.

References

1. L. Hao, X. Li, L. Zhi, *Adv. Mater.* **25**, 3899 (2013)
2. A.L.M. Reddy, S.R. Gowda, M.M. Shaijumon, P.M. Ajayan, *Adv. Mater.* **24**, 5045 (2012)
3. S. Selvam, B. Balamuralitharan, S.N. Karthick, A.D. Savariraj, K.V. Hemalatha, S.-K. Kim, H.-J. Kim, *J. Mater. Chem. A* **3**, 10225 (2015)
4. G.A. Snook, P. Kao, A.S. Best, *J. Power Sources* **196**, 1 (2011)
5. G. Wang, L. Zhang, J. Zhang, *Chem. Soc. Rev.* **41**, 797 (2012)
6. Z.-S. Wu, G. Zhou, L.-C. Yin, W. Ren, F. Li, H.-M. Cheng, *Nano Energy* **1**, 107–131 (2012)
7. E. Frackowiak, *Phys. Chem. Chem. Phys.* **9**, 1774 (2007)
8. Y. Shao, M.F. El-Kady, L.J. Wang, Q. Zhang, Y. Li, H. Wang, M.F. Mousavi, R.B. Kaner, *Chem. Soc. Rev.* **44**, 3639 (2015)
9. L.L. Zhang, X.S. Zhao, *Chem. Soc. Rev.* **38**, 2520 (2009)
10. X. Zhang, H. Zhang, C. Li, K. Wang, X. Sun, Y. Ma, *RSC Adv.* **4**, 45862 (2014)
11. O. Barbieri, M. Hahn, A. Herzog, R. Kotz, *Carbon* **43**, 1303 (2005)
12. Y. Zhu, S. Murali, M.D. Stoller, K.J. Ganesh, W. Cai, P.J. Ferreira, A. Pirkle, R.M. Wallace, K.A. Cychosz, M. Thommes, D. Su, E.A. Stach, R.S. Ruoff, *Science* **332**, 1537 (2011)
13. X. Chia, A.Y.S. Eng, A. Ambrosi, S.M. Tan, M. Pumera, *Chem. Rev.* **115**, 11941 (2015)
14. M. Pumera, Z. Sofer, A. Ambrosi, *J. Mater. Chem. A* **2**, 8981 (2014)
15. S. Stankovich, D.A. Dikin, R.D. Piner, K.A. Kohlhaas, A. Kleinhammes, Y. Jia, Y. Wu, S.T. Hguyen, R.S. Ruoff, *Carbon* **45**, 1558 (2007)
16. G. Xiong, P. He, L. Liu, T. Chen, T.S. Fisher, *J. Mater. Chem. A* **3**, 22940 (2015)
17. M. Zhi, C. Xiang, J. Li, M. Li, N. Wu, *Nanoscale* **5**, 72 (2013)
18. Z. Luo, J. Zhou, L. Wang, G. Fang, A. Pan, S. Liang, *J. Mater. Chem. A* **4**, 15302–15308 (2016)
19. L. Ma, L. Xu, X. Zhou, X. Xu, L. Zhang, *RSC Adv.* **6**, 91621–91628 (2016)
20. M. Lee, S.K. Balasingam, H.Y. Jeong, W.G. Hong, H.-B.-R. Lee, B.H. Kim, Y. Jun, *Sci. Rep.* **5**, 8151 (2015)
21. A. Ramadoss, S.J. Kim, *Carbon* **63**, 434 (2013)
22. A. Muthukannan, J. Henry, K. Mohanraj, G. Sivakumar, S. Thanikaikarasan, *J. Mater. Sci.: Mater. Electron.* **27**, 9947–9952 (2016)
23. C.K. Chua, M. Pumera, *J. Mater. Chem.* **22**, 23227 (2012)
24. M.T.H. Aunkor, I.M. Mahbukul, R. Saidur, H.S.C. Metselaar, *RSC Adv.* **5**, 70461 (2015)

25. Y. Shi, C. Hua, B. Li, X. Fang, C. Yao, Y. Zhang, Y.-S. Hu, Z. Wang, L. Chen, D. Zhao, G.D. Stucky, *Adv. Funct. Mater.* **23**, 1832 (2013)
26. M.A. Bissett, I.A. Kinloch, R.A.W. Dryfe, *ACS Appl. Mater. Interfaces* **7**, 17388 (2015)
27. Q. Cheng, J. Tang, J. Ma, H. Zhang, N. Shinya, L.-C. Qin, *Phys. Chem. Chem. Phys.* **13**, 17615 (2011)
28. Q. Cheng, J. Tang, J. Ma, H. Zhang, N. Shinya, L.-C. Qin, *Carbon* **49**, 2917 (2011)
29. S.K. Balasingam, A. Thirumurugan, J.S. Lee, Y. Jun, *Nanoscale* (2016). <https://doi.org/10.1039/C6NR01200K>
30. J. Yan, Z. Fan, T. Wei, W. Qian, M. Zhang, F. Wei, *Carbon* **48**, 3825 (2010)
31. W. Zhang, H. Lin, Z. Lin, J. Yin, H. Lu, D. Liu, M. Zhao, *ChemSusChem* **8**, 2114 (2015)